World Applied Sciences Journal 33 (9): 1440-1445, 2015
ISSN 1818-4952

DOI: 10.5829/idosi.wasj.2015.33.09.288

Analysis of Optical Pulse's Position Effect on Temporal Response Characteristics of GaAs Metal-Semiconductor-Metal Photodetector

[1]Atefeh Habibpour and [2]Narottam Das

[1]Department of Physics, Kazerun Branch, Islamic Azad University, Kazerun, Iran
[2] School of Mechanical and Electrical Engineering,
University of Southern Queensland, Toowoomba, QLD 4350, Australia

Abstract: Photocurrents in a GaAs metal-semiconductor-metal (MSM) photodetector have been numerically modelled as a function of optical pulse's position in a one-dimensional structure using Ambipolar transport theory and discrete Fourier transform method. The modelled results represent the carriers' concentrations as well as the maximum value of the photocurrents that pass through the device when the optical pulse position changes on the device active region (i.e., the region between two top contacts). The simulation has been performed at low level injection of the excess carriers (i.e., photo-carriers) and with no bias voltage applied to the photodetector in equilibrium condition. The numerical simulation results show that for optical pulse position in the cathode region, the magnitude of the photocurrent is exactly the same but opposite direction of the anode region. The response of the photodetector is 'zero' when a pulse is positioned at the center of the active region. This important feature of the device could make it attractive for micro-scale positioning of high sensitive devices. The modelled results are qualitatively agreed with the experimentally observed behavior of the device.

Key words: Ambipolar transport theory · Discrete Fourier transform method · Equilibrium condition · Metal-semiconductor-metal (MSM) photodetector · Numerical modelling

INTRODUCTION

The planar metal-semiconductor-metal (MSM) photodetectors are important components in optical communication systems due to their ease of fabrication, compatibility with field effect transistors and high speed operations [1]. The MSM photodetectors have extensive applications, including optical fiber communications, optical sampling and optical interconnects [2]. Most of the useful photodetector devices are based on the MSM structures due to their simplicity of configuration. The MSM configuration shows a very low dark current due to the rectifying nature of the contacts and the high resistivity of the material [3]. A simple schematic diagram of an MSM photodetector is shown in Figure 1. An MSM consists of a semiconductor absorbing layer on which two electrodes have been deposited to form a back-to-back Schottky diode. In the photodetector, the photocarriers are generated inside the intrinsic region (i.e., I-region) when optical pulses are incident on the device. Then, these photocarriers can be collected by the contacts of the phtodetector and result in a photocurrent. Increasing the illumination intensity of the optical pulses are hitting on the surface of the semiconductor would increase the number of electron-hole pairs inside the semiconductor slab and hence results in the increase of photocurrent. The MSM photoconductor can operate without an external field, which is also called an equilibrium condition, if the photocarriers have sufficient mobility and lifetime to reach the Ohmic contacts for the collection. Otherwise, an external field is usually provided to move the charge photocarriers through the material.

Experimentally in the equilibrium condition, the GaAs MSM photodetector shows different temporal responses, when the position of the optical pulse changes on the surface of the active region (i.e., I-region). For equal distances of laser spots from the center of the I-region, the temporal response of the device is symmetric. The temporal response vanishes when the laser spot hits the center of the I-region as shown in Figure 2 [4].

Corresponding Author: Atefeh Habibpour, Department of Physics, Kazerun Branch, Islamic Azad University, Kazerun, Iran. Fax: +9842230508.

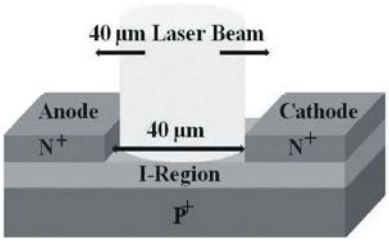

Fig. 1: Schematic picture of a 40 µm gap GaAs MSM photodetector and a 40 µm and 580 nm beam spot of a dye laser impinging upon the device surface

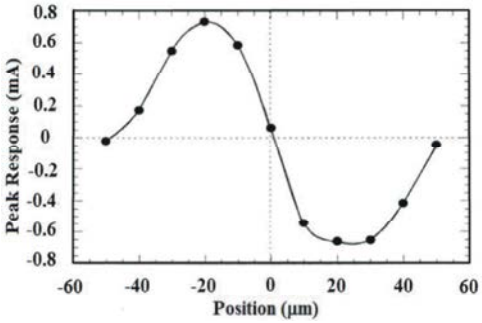

Fig. 2: Experimental results of peak response as a function of beam position on a 40 µm gap I-region with '0' (zero) voltage [4]

We used Ambipolar transport theory to describe the behavior of photogenerated carriers in the active region [5]. Here, we assume that the photogenerated carriers are injected in the low level injection condition. We have applied a discrete Fourier transform (DFT) method to solve the Ambipolar transport equation numerically. We have used a spatially variable optical pulse as the initial condition. The result of this simulation shows that the responses of the photodetector are asymmetric around the centre of the I-region. In other words, the direction and magnitude of electrical responses of the device for an optical pulse position in the region between the central point of the I-region and one of the two contacts are opposite to that of optical pulse position in the center point of the I-region and the other contact. The response of the device to the optical pulse position at the centre of the I-region is zero.

In earlier work, we reported how the impulse response of an MSM photodetector depends on the position of the laser beam on the active region (I-region), when an external voltage is applied to the device. In fact, the peak response of the photodetector increases by moving the laser spot from the cathode region toward the anode region.

Analysis of Carrier Transport in MSM Photodetector: An MSM photodetector can be modelled as a one dimension (1-D) structure [7-9]. This approach can easily be justified if the absorption depth δ of an incident photon was much less than the I-region length L (i.e., $\delta \ll L$), so that the curvature of the electric field lines between the two contacts is small, while the field is approximately constant. To estimate the absorption depth of a typical GaAs MSM structure, we assume that the optical power at depth z in the I-region is given by [10],

$$p(z) = p_{inc}.(1-R).e^{-\alpha z} \tag{1}$$

where, p_{inc} is the incident power and R and α are the reflection and absorption coefficients, respectively. By assuming normal incident, the reflection coefficient R can be calculated from the following equation [11],

$$R = \frac{(n-1)^2 + k^2}{(n+1)^2 + k^2} \tag{2}$$

where, n and k are the refractive index and absorption constant, respectively. The absorption constant k is related to the absorption coefficient α through the following equation,

$$k = \frac{\alpha\lambda}{4\pi} \tag{3}$$

For visible light around the wavelength of λ = 580 nm, the refractive index *n* and absorption coefficient α, for GaAs are 3.34 and 59841, respectively. By substituting these values into the above equation (3) and then putting the result in the equation (2), the reflection coefficient is calculated as R = 0.291. Then for a given optical power, p_{inc}, the absorption depth at which 1/e times of the optical power has been absorbed is found to be 0.11 µm, which is much smaller than the I-region length, L=40 µm and therefore the structure can be modelled in 1-D.

When an optical pulse hits the I-region, excess electrons δn in the conduction band and excess holes δp in the valence band are created in addition to the thermal equilibrium concentrations, n_0 and p_0.

Using Ambipolar theory results in determining the carrier densities, as well as the photocurrents in different initial conditions, which are mainly determined by the position of the optical pulse relative to the I-region surface. The time-dependent Ambipolar continuity equation for electrons and holes in 1-D and in the absence of an external field has the following formula [5-6], [12],

$$D'\frac{\partial^2(\partial n)}{\partial x^2}+g-R=\frac{\partial(\partial n)}{\partial t} \quad (4)$$

where $\delta n(x,t) \approx \delta p(x,t)$ and D' is the Ambipolar diffusion coefficient and is defined as,

$$D'=\frac{D_n D_p(n+p)}{D_n n+D_p p} \quad (5)$$

$$p = p_0 + \delta p \quad (6)$$

$$n = n_0 + \delta n \quad (7)$$

where, p and n are total carrier concentrations. The intrinsic region of the device is a low p type GaAs. In these simulations, a shallow acceptor concentration p_0 of 2×10^{20} m^{-3} and donor concentration n_0 of 0.5×10^{20} m^{-3} are chosen to give an equilibrium hole density p_l of 1×10^{20} m^{-3} in the active region in agreement with the parameters of the actual device. The diffusion coefficients are related to the mobilities by the Einstein relation [13-15],

$$D_{n,p}=\frac{kT}{e}\mu_{n,p} \quad (8)$$

where, k is the Boltzmann's constant and T is the carrier temperature (room temperature). Carriers' mobility μ_n and μ_p were determined via their dependence on the doping level in the I-region. Thus, the carriers' mobilities μ_n and μ_p are equal to 8000 $cm^2.s^{-1}.v^{-1}$ and 400 $cm^2.\ s^{-1}.\ v^{-1}$, respectively [16].

The parameter g is the generation rate of the excess carriers in the I-region. Since the time period of the optical pulse is very short about 5 ps, we can consider generation only happen at t=0 and, besides, there is no generation in latter time steps. Here, it is assumed that the laser pulse has a peak height equivalent to the band-to-band generation rate of $\approx 2 \times 10^{23}$ (electron-hole).$m^{-3}.s^{-1}$ at the illumination surface. Considering the time period of the optical pulse, it gives a peak electron and hole density of 1×10^{12} m^{-3} in the active layer. The laser spot size has been specified as 40 μm diameter.

The parameter R is the recombination rate of the excess carriers and it is modelled using the Shockley–Read–Hall (SRH) equation as given by [17-18],

$$R=\frac{(pn-n_i^2)}{\left[\tau_p\left(n+n_i\exp(\frac{E_{trap}}{kT})\right)+\tau_n\left(p+n_i\exp(-\frac{E_{trap}}{kT})\right)\right]} \quad (9)$$

where, n and p are the total electron and hole densities, E_{trap} is the deference between the defect level and the intrinsic level, n_i denotes effective intrinsic density and τ_n and τ_p are SRH lifetime of electrons and holes respectively, which are assumed to be 0.1 and 0.3 ns in the same order.

Simulation Method: We have used the DFT method to simulate the device responses to the beam of laser pulses hitting different locations between the two contacts. For this purpose, we first Fourier transform the entire Ambipolar equation (4) [19-21].

Here, the excess carrier densities are taken to be zero at the contacts. This implies an infinite surface recombination velocity at the contacts [22]. By considering this boundary condition, the Fourier Transform of the spatial derivative becomes,

$$F[\frac{\partial^2(\delta n(x,t))}{\partial x^2}]=(ik)^2F[\delta n(x,t)] \quad (10)$$

Also the Fourier Transform of the time derivative is equal to,

$$F[\frac{\partial(\delta n(x,t))}{\partial t}]=\frac{\partial}{\partial t}F[\delta n(x,t)] \quad (11)$$

where, the term $F[\delta n(x, t)]$ is the Fourier transform of the excess carrier concentration and it is conventionally represent via $\delta N(k,t)$. In fact, this term is the carrier concentration in k-space. Finally, after applying the DFT method to solve numerically the equation (4) [19], [23-25], $\delta N(k,t)$ obtains. At the end, in order to obtain the excess carrier concentration in x-space $\delta n(x,t)$, we have to take the Inverse Fourier Transform of $\delta N(k,t)$.

In the simulation process, we chose 2N = 512 sample points in both x-space and k-space. The values of sample points x_n and k_j satisfy the following formulas,

$$x_n=\frac{nL}{2N},\quad 0\le n\le(2N-1) \quad (12)$$

$$k_j=\frac{2\pi j}{L},\quad 0\le j\le(2N-1) \quad (13)$$

where, n and j are the integers.

RESULTS AND DISCUSSION

This section discussed the simulation results in details. Figure 3 shows the plots of normalized carriers density versus the length of the I-region at time t = 0, 40

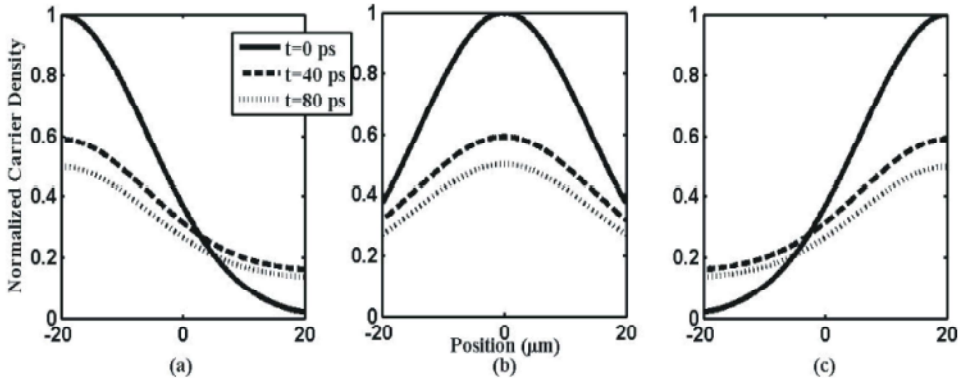

Fig. 3: Normalized carrier density versus optical pulse position at times t = 0, 40 and 80 picoseconds, when the pulse position is at -20 (Figure 3(a)), 0 (Figure 3(b)) and 20 μm (Figure 3(c)), respectively. The photodetector is in the equilibrium condition

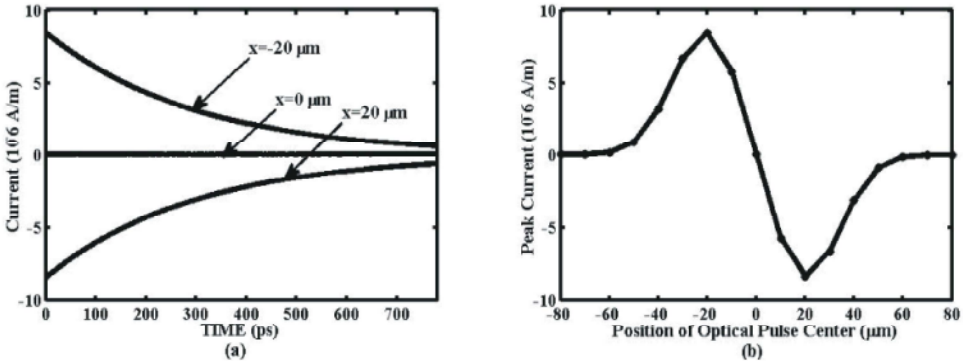

Fig. 4: (a) The photocurrent for the optical pulse position at -20 (upper curve), zero (middle curve) and 20 μm (lower curve). (b) The peaks of photocurrents as a function of beam position on a 40 μm gap I-region. Device is in the equilibrium condition

and 80 ps, respectively. The normalized carrier density for optical pulse positions at -20, 0 and 20 μm are shown in Figure 3(a), Figure 3(b) and Figure 3(c), respectively. From these plots, it is evident that the diffusion of photocarriers results in a spread of the initial profile. Also, due to the recombination process, the initial photocarriers' peak decreases with time.

Finally the carrier densities are integrated over the length L between the two top contacts of the photodetector to yield the photocurrent due to the carriers' diffusion in the semiconductor. The diffusion current can be calculated from the general form given by [9],

$$I(t) = \frac{dQ}{dt} = \frac{e}{L}\int_0^L D' \frac{\partial(\delta n(x,t))}{\partial x} dx \qquad (14)$$

In equation (14), the term of $\frac{\partial(\delta n(x,t))}{\partial x}$ is in fact the slope of the photo-carriers density curve and the integral means adding up all possible quantities for this term over the I-region. Obviously, this term can possess a negative quantity as well as a positive quantity and consequently it can cause overall a negative or positive photocurrent depending on the values which are added up. The photocurrent for the optical pulse position at -20 (upper curve), zero (middle curve) and 20 μm (lower curve) is shown in Figure 4(a). Also, the maximum value of the photocurrent versus the position of the optical pulse on the I-region is shown in Figure 4(b).

It can be seen from Figure 4 that the photocurrent of the photodetector for optical pulse position in cathode region is equal but opposite sign to that of the anode region. In fact, in the absence of a biased voltage, this device behaves completely symmetrical. Depending on the optical pulse centre is near to which contact, more photocarries diffuse towards this contact and cause to a specific photocurrent. So, the simulated results show that the magnitude and the direction of the photocurrents depend on the position of the optical pulse's centre.

CONCLUSION

In conclusion, we have developed a one-dimensional simulation program based on the diffusion model and discrete Fourier transform (DFT) method in order to demonstrate the behavior of the GaAs MSM photodetector in the equilibrium and low level injection condition. The model has been applied to comprehensively investigate the photogenerated carriers' concentrations as well as the electrical responses of the device. The simulated results reveal the dependence of the electrical response with the optical pulse position. This dependence can be enormously useful in the design of MSM photodetector for operation in equilibrium condition. The obtained results in this simulation are qualitatively in agreement with the experimental results.

REFERENCES

1. Rong-Heng Yuan, Jia-Lin Shieh, *et al*., 1995. GaAs Metal-Semiconductor-Metal Photodetectors (MSM-PD's) with ALGaAs Cap and Buffer Layer. Journal of Chinese Institute of Engineering, 18(3): 445-449.
2. Das, N.K., A. Karar, C.L. Tan, M. Vasiliev, K. Alameh and Y.T. Lee, 2011. Metal-Semiconductor-Metal (MSM) Photodetectors with Plasmonic Nanogratings. Pure and Applied Chemistry, 83(11): 2107-2113.
3. Müller, A., *et al*., 2008. Ultraviolet MSM Photodetector Based On GaN Micromachining. In the Proceedings of the 2008 Romania International Semiconductor Conference, pp: 91-94.
4. Mashayekhi, H.R., 1999. Theoretical and Experimental Studies of Back-Gated Metal-Semiconductor-Metal Photodetectors. Doctor of Philosophy Dissertation, University of Essex, Department of Physics, UK.
5. Neaman, D.A., 2003. Semiconductor Physics and Devices: Basic Principles. 3rd ed., McGraw-Hill, Inc.
6. Habibpour, A. and H.R. Mashayekhi, 2011. Numerical Modeling of the Effect of Optical Pulse Position on the Impulse Response of a Metal-Semiconductor-Metal (MSM) Photodetector (Low Field Condition). The European Physical Journal Applied Physics, 55: 10502.
7. Ch, S. Harder, B.J. Van Zeghbroeck, M.P. Kesler, H.P. Meier, P. Vettiger, D.J. Webb and P. Wolf, 1990. High Speed GaAs/AlGaAs Optoelectronic Devices for Computer Applications. IBM Journal of Research and Development, 34(4): 568-584.
8. Koscielniak, W.C., J.L. Pelouard and M.A. Littlejohn, 1989. Dynamic Behavior of Photocarriers in a GaAs Metal-Semiconductor-Metal Photodetector with Sub-Half-Micron Electrode Pattern. Applied Physics Letter, 54: 567-569.
9. Sarto, A.W. and B.J.V. Zeghbroeck, 1997. Photocurrents in a Metal-Semiconductor-Metal Photodetector. IEEE Journal of Quantum Electronics, 33(12): 2188-2194.
10. Wood, D., 1994. Optoelectronic Semiconductor Devices. Prentice Hall international limited.
11. Blackemore, J., 1982. Semiconducting and Major Properties of Gallium Arsenide. Journal of Applied Physics, 53(10): r137.
12. Wurfel, P., 2005. Physics of Solar Cells. WILY-VCH Verlay GmbH & Co. KGaA, Weinheim.
13. Seeger, K., 1982. Semiconductor Physics. 2nd ed., New York: Springer.
14. Tarik Asar, Suleyman Ozcelik, *et al*., 2014. Structural and Electrical Characterizations of $In_xGa_{1-x}As$/InP Structures for Infrared Photodetector Applications. Journal of Applied Physics, 115: 104502.
15. Smith, R.A., 1978. Semiconductors. 2nd ed., New York: Cambridge University Press.
16. Bhattacharya, P., 1994. Semiconductor Optoelectronic Devices. Prentice Hall, Inc.
17. Chen Bin, *et al*., 2010. Simulation and Optimization of a 6H-SiC Metal-Semiconductor-Matal Ultraviolet Photodetector. Journal of Semiconductors, 31(6): 064010(1-5).
18. Zehor Allam, *et al*., 2013. The Electrical Properties of InGaN/GaN/AlN MSM Photodetector with Au Contact Electrodes. Journal of Electron Devices, 17: 1476-1485.
19. Brigham, E.O., 1988. The Fast Fourier Transform and Its Applications. Prentice-Hall, Inc.
20. Haberman, R., 1987. Elementary Applied Partial Differential Equations with Fourier Series and Boundary Value Problems. 2nd ed., Prentice-Hall Inc.
21. Habibpour, A. and H.R. Mashayekhi, 2011. Numerical Modeling of the Transient Response of Metal-Semiconductor-Metal Photodetector Using Discrete Fourier Transform Method. In the Proceedings of the 2011 IOP Condensed Matter and Materials Physics Conference (CMMP10), 286.
22. Iverson, A.E. and D.L. Smith, 1987. Mathematical Modeling of Photodetector Transient Response. IEEE Transactions on Electronic Devices, 34(10): 2098.

23. James, J.F., 2004. A Student's Guide to Fourier Transforms with Applications in Physics and Engineering. Cambridge University Press.
24. Quarteroni, A. and F. Saleri, 2006. Scientific Computing with Matlab and Octave. 2nd ed., Springer-Verlag Italian.
25. Wilson, H.B., L.H. Turcotte and D. Halpern, 2003. Advanced Mathematics and Mechanics Applications Using Matlab. 3rd ed., Chapman & Hall/CRC.